

Disentangling Instrumental Features of the 130 GeV Fermi Line

Daniel Whiteson¹

¹*Department of Physics and Astronomy, University of California, Irvine, CA 92697*

We study the instrumental features of photons from the peak observed at $E_\gamma = 130$ GeV in the spectrum of Fermi-LAT data. We use the SLOTS algorithm to reconstruct – separately for the photons in the peak and for background photons – the distributions of incident angles, the recorded time, features of the spacecraft position, the zenith angles, the conversion type and details of the energy and direction reconstruction. The presence of a striking feature or cluster in such a variable would suggest an instrumental cause for the peak. In the publically available data, we find several suggestive features which may inform further studies by instrumental experts, though the size of the signal sample is too small to draw statistically significant conclusions.

PACS numbers:

INTRODUCTION

While the existence of dark matter is widely accepted, its particle nature remains undiscovered. Potential avenues for discovery include observation of production at high energy accelerators, scattering with heavy nuclei in large low-noise underground volumes, or annihilation.

A clear signal of dark matter annihilation may be carried by gamma rays traveling to Earth from regions in the galaxy of high dark-matter density. As they do not typically scatter after their production, the photon energy and direction are powerful handles for understanding the mechanism of dark matter annihilation into standard model particles.

One mechanism is annihilation resulting in quarks, which would hadronize and yield π^0 particles which in turn produce photons. The spectrum of such a process would give fairly low energy photons ($E_\gamma \leq \approx 50$ GeV) which may be difficult to distinguish from other sources.

A more striking feature may appear from annihilation directly into two-body final states including a photon. Rather than yielding a broad energy spectrum, this process would produce a photon with a well-defined energy given (for the process $\chi\chi \rightarrow \gamma Y$) by

$$E_\gamma = m_\chi \left(1 - \frac{M_Y^2}{4m_\chi^2} \right) \quad (1)$$

where M_Y is the mass of the second annihilation product, such as a Z boson or a second photon. For the case where $Y = \gamma$, the line occurs at the mass of the dark matter particle, $E_\gamma = m_\chi$. This makes a search for peaks in the photon spectrum an important component of the dark matter program using Fermi-LAT data [1, 2].

Recent studies have identified a feature in the gamma ray spectrum near $E_\gamma = 130$ GeV [3, 4] with a source close to the galactic center [3–6]. The line feature is not accompanied by a lower-energy continuum emission, as would be expected in many models of dark matter interaction [7]. However, the large apparent significance

of the feature has generated keen interest in exploring other, more mundane explanations, such as unconsidered features in the non-dark-matter background in the difficult region of the galactic center, or instrumental effects in the Fermi-LAT detector.

In this paper, we present a first study of the instrumental characteristics of photons in the line feature, using the SLOTS [8] algorithm to disentangle the two populations (background and peak). This allows us to reconstruct distributions in variables which may reveal instrumental issues that would not otherwise be apparent.

SLOTS

In a sample of events with multiple sources, if one variable can be used to discriminate between the sources, the SLOTS algorithm can reconstruct the statistical distribution of each of the sources in other variables, which we refer to as the ‘unfolding variables’. SLOTS uses only information from the discriminating variable and knowledge of the probability density functions (pdf) for each source in the discriminating variable. In addition, the algorithm assumes that the pdfs can be factorized between the discriminating and unfolding variables.

For the purposes of clarity, we simplify the general SLOTS formalism of Ref. [8] into the two-sources case we will apply to the Fermi-LAT data.

Given pdfs for two sources $f_1(y)$, and $f_2(y)$ in the discriminating variable y , one can construct a histogram in another unfolding variable x using weights for each source class, sP_1 and sP_2 , defined as:

$$sP_1(y) = \frac{\mathbf{V}_{11}f_1(y) + \mathbf{V}_{12}f_2(y)}{N_1f_1(y) + N_2f_2(y)}$$

$$sP_2(y) = \frac{\mathbf{V}_{21}f_1(y) + \mathbf{V}_{22}f_2(y)}{N_1f_1(y) + N_2f_2(y)}$$

where N_1 and N_2 are the number of events in each class, as extracted by a likelihood fit of f_1 and f_2 to the observed distribution in y , and the inverse of the matrix \mathbf{V} is a symmetric 2×2 matrix defined as

$$\mathbf{V}_{ab}^{-1} = \sum_{i=1}^N \frac{(N_1 + N_2)f_a(y_i)f_b(y_i)}{(N_1f_1(y_i) + N_2f_2(y_i))^2}$$

A histogram h in the unfolding variable x can then be constructed for source 1 as

$$h_i = \sum_{j=1}^{N_i} sP_1(y_{ji})$$

where i is the bin index in the x variable, N_i is the number of events in that bin, and y_{ji} is the value of the y variable for the j th event in the i th bin. A histogram for source 2 would be constructed by replacing $sP_1 \rightarrow sP_2$.

This technique is superior to simply making a selection in the y variable to enhance the relative contribution of one source, which may still be significantly polluted by the other source. Note that if the two sources were completely separable in the y variable, then the sPlot weights would reduce trivially to 0 or $1/N$. This appears to be the first application of this algorithm to an astrophysical problem [9].

Example of sPLOTS in Toy Data

As an illustrative example, we generate toy data from two sources according to the pdfs:

$$f_{\text{peak}}(x, y) = \frac{1}{\sqrt{2\pi}} e^{-\frac{1}{2}(y-5)^2} \times \frac{10-x}{50}$$

and

$$f_{\text{non-peak}}(x, y) = \frac{x}{50}$$

where $f_{\text{peak}}(x, y)$ is normally distributed in y with $\sigma = 1$, while $f_{\text{non-peak}}(x, y)$ is uniform in y , providing good discrimination power. Our goal is to construct histograms which reveal the distribution in x for each of the two sources.

Figure 1(a) shows the generated event distribution in the discriminating variable y and the unfolding variable x using 1000 events from each source. Figure 1(b) shows the projection in y and the result of the fit to extract N_1 and N_2 , which uses only this one-dimensional projection and the y -dependence of the pdfs.

The unfolded distributions for each source are shown in Figure 1(c,d), along with the true pdfs in x , which

were not used in reconstructing the unfolded distributions. The sPLOTS algorithm is successfully able to disentangle the two sources and reveal the x -dependence of each.

Note that since the distributions use a statistical unfolding (rather than event-by-event) and is unaware of physical constraints, it is possible to have a negative prediction in a bin. The statistical uncertainty in a given bin is $\Delta N = \sqrt{\sum_i sP^2}$.

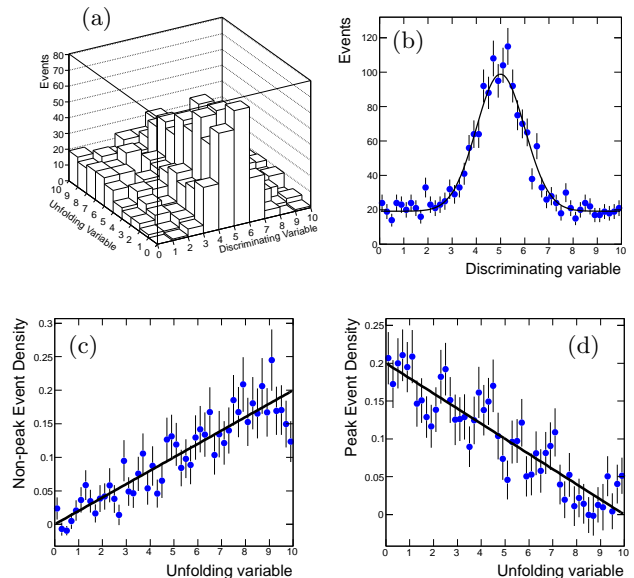


FIG. 1: Example application of the sPLOTS [8] algorithm in toy data. Top left, distribution of toy data in the discriminating and unfolding variable. Top right, distribution of peak and non-peak events in the discriminating variable, with the fitted combined pdf. Bottom left (right) shows the non-peak (peak) distribution in the unfolding variable (blue points), with the true pdf (black line). The unfolded distributions are calculated by sPLOTS using only information from the discriminating variable.

The unfolded distributions can be reconstructed just as well for non-linear pdfs, see the example in Fig. 2(a,b), where trigonometric functions have replaced the x dependence of the pdfs.

Correlations between x and y in the pdfs can lead to biases, but do not catastrophically undermine the unfolding. For example, if we use

$$f_{\text{non-peak}}(x, y) = \frac{y + (1 - y/5)x}{50}$$

so that the slope in x varies from positive to negative over $y \in [0, 10]$:

$$f_{\text{non-peak}}(x, 0) = \frac{x}{50}, f_{\text{non-peak}}(x, 10) = \frac{10-x}{50},$$

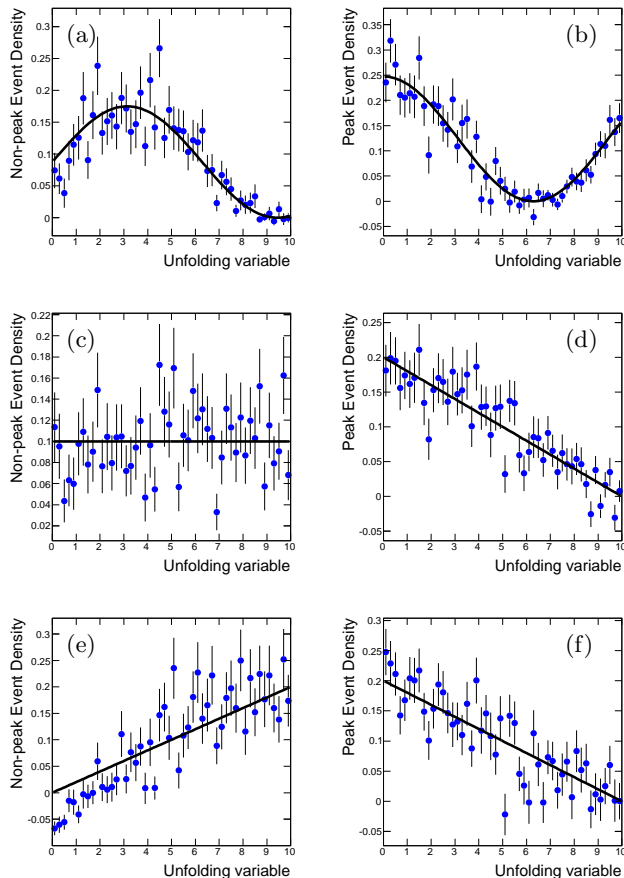


FIG. 2: Tests of the robustness of sPLOTS. In each case, blue points show the sPLOTS reconstructed distribution and the black line is the true pdf. Top, reconstruction of the unfolding variable with non-linear pdfs. Center and bottom, impact of correlations in the pdfs on the reconstruction of the unfolding variable. Center uses a slope which varies with the discriminating variable, averaging to zero. Bottom uses a variable-width peak. See text for details.

then sPlots recovers the average x dependence for the non-peak source, see Fig. 2(c,d), and the correct dependence for the events from the peak.

If instead the width of the peak in y varies with x , there may be some biases introduced, but the effects are minor, even for a doubling of the peak width over the range $y \in [0, 10]$, see Fig 2(e,f).

Note that these types of correlations would be even more troublesome for the traditional strategy of making a selection to enhance or suppress one source.

THE FERMI-LAT DATA SAMPLE

We use the publically available data with the extended photon data from the Fermi-LAT collaboration through June 28th, 2012, making standard quality re-

quirements [10] and examining a square region around the galactic center, with galactic longitude $-5 < l < 5$ degrees and galactic latitude $-5 < b < 5$ with energy greater $E_\gamma \geq 50$ GeV.

Other than the reconstructed energy, the photons have other measured characteristics [13] which may give insight into instrumental effects:

- incident angle θ , measured with respect to the top-face normal of the LAT,
- azimuth angle ϕ , measured with respect to the top-face normal of the LAT, folded as described in Eq. (15) of Ref. [11].
- zenith angle, measured with respect to the zenith line, which passed through the earth and LAT's center of mass,
- earth azimuth angle, the azimuthal angle relative to the same line as the zenith, defined such that zero indicates the photon came from the northern direction,
- mission elapsed time, measured relative to January 1, 2001,
- conversion type (front or back), indicates whether the event induced pair production in the front (thin) layers or the back (thick) layers of the tracker,
- the probability that the best energy chosen from the three energy estimators is correct,
- the probability that the direction estimate is good,
- ratio of true/raw energy,
- first layer of the tracker with a hit,
- the magnetic field in which the LAT is immersed, as parameterized by the McIlwain B and L parameters [14],
- the distance from the center of the South Atlantic anomaly, calculated as $\sqrt{\Delta\text{long}^2 + \Delta\text{lat}^2}$ in terms of Earth latitude and longitude, and
- the geomagnetic latitude of the spacecraft.

In this paper, we study the distribution in these variables for signal-like and background-like photons. In some cases, a large difference in the distribution of signal-like and background-like photons would be a clear indication of an instrumental issue. This is especially true for variables related to the spacecraft position, environment or angle (mission time, magnetic field, earth azimuth angle, distance from the SA anomaly, geomagnetic latitude). Other variables are connected to the quality or class of the reconstruction (incident angles, conversion

type, reconstruction details) and would give more subtle clues as to whether the feature is due to a sub-class of photons, or photons with particularly high or poor resolution. The response of the LAT is dependent on some of these variables. For example, the energy resolution is a function of the incident angle θ and the conversion type, see Fig. 3. In addition, the point-spread function depends on the point in the LAT where the photon converts.

These indications would be only the first clues, and would need detailed follow-up by the instrument experts; a complete study is not possible in the information available in the public data. The Fermi-LAT collaboration has already performed detailed studies of the instrument performance and calibration, including studies of potential systematic biases [11, 15, 16].

Single-Line Analysis

To analyze the features of the Fermi-LAT data using SLOTS, we must define background and signal pdfs in the discriminating variable, E_γ . The background pdf is a simple power-law:

$$f_{\text{bg}}(E_\gamma|\beta, \alpha) = \beta \left(\frac{E_\gamma}{E_0}\right)^{-\alpha}$$

For the observed feature we assume a single line (the two-line hypothesis is discussed below) where the pdf $f_{\text{line}}(E_\gamma|E_{\text{line}})$ is defined according to the Fermi-LAT energy dispersion tools definition [12] with a true photon energy of E_{line} , see Fig. 3. Applying these pdfs to the observed photon energy spectrum yields the fit seen in Fig. 4.

Unfolded distributions of incidence angles are shown in Fig. 5. The distributions in galactic coordinates can be seen in Fig. 6. Zenith and azimuthal angle distributions are in Fig. 7, and the recorded time and conversion type are in Fig. 8. Energy and direction reconstruction quality are in Fig. 9 and the reconstructed/raw energy ratio as well as the first layer of the tracker with a hit are shown in Fig. 10. The magnetic field parameters are shown in Fig. 11 and the distance from the South Atlantic anomaly and the geomagnetic latitude are shown in Fig. 12.

In each case, we compare the distributions quantitatively by calculating the χ^2/dof between the peak and background distributions, shown in Table I. As the signal and background weights are anti-correlated, this is calculated as

$$\chi^2 = \sum_{\text{bin } i} \frac{(N_{\text{peak}}^i - N_{\text{bg.}}^i)^2}{(\Delta N_{\text{peak}}^i + \Delta N_{\text{bg.}}^i)^2}$$

where N_{peak}^i is the sum of the weights $\sum sP_{\text{peak}}$ in that bin, and ΔN_{peak}^i is calculated from toy simulations which

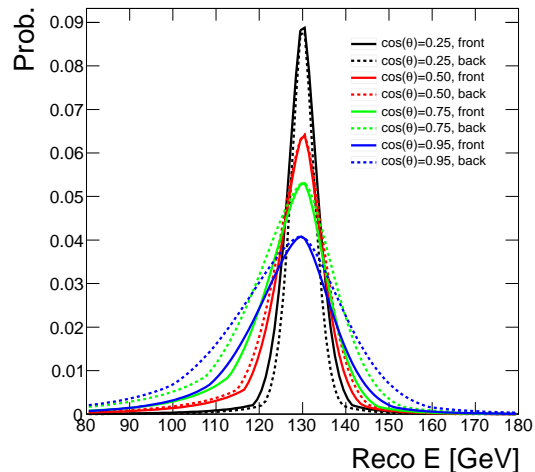


FIG. 3: Probability density function in Fermi-LAT reconstructed photon energy for photons with true energy of $E_\gamma = 130$ GeV, for varying choices of the incident angle θ and the conversion type [12].

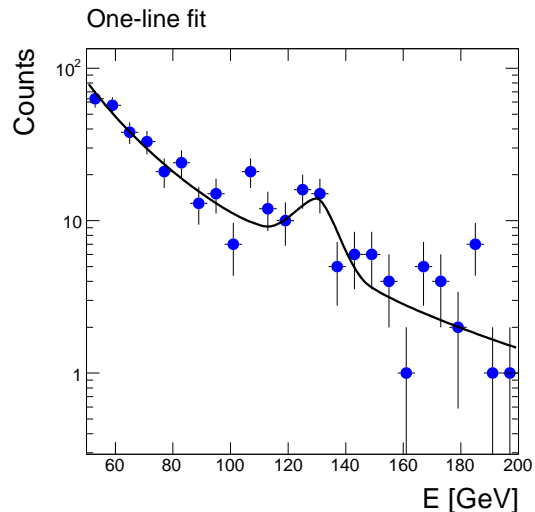


FIG. 4: Energy of Fermi-LAT photons with signal plus background fit, using a single-line hypothesis at $E_\gamma = 130$ GeV.

estimate the expected variance of the measurement in each bin. Similar expressions apply for the background uncertainties.

Double-Line Analysis

It has been suggested [17] that there may be two photon lines, the $\gamma\gamma$ feature being accompanied by a feature due to γZ production, which would be at lower E_γ (see Eq (1)).

We modify the signal pdf to include two lines, one at

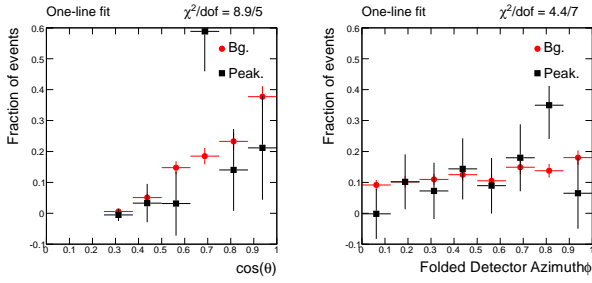


FIG. 5: Disentangled signal and background distributions. Left, $\cos(\theta)$ where θ is the photon incidence angle relative to a line normal the Fermi-LAT face. Right, ϕ , the photon incidence angle relative to the sun-facing side [13].

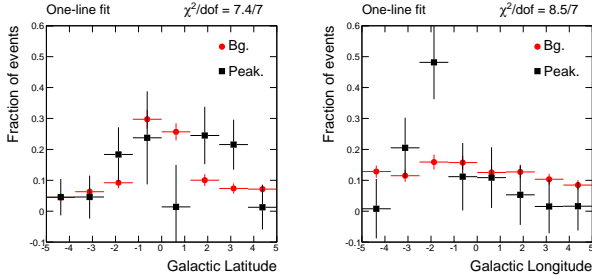


FIG. 6: Disentangled signal and background distributions in galactic coordinates, b (latitude) and l (longitude) [13]. No smoothing has been applied.

110 GeV and one at 130 GeV (the results are not sensitive to the precise position of the second line). We allow the two line features to float independently, but in the sPLOTS analysis we treat them together as a single pdf once their relative normalization has been fixed by the fit. The result of the fit can be seen in Figure 13. Note, however, that systematic or instrumental issues which cause features in the energy spectrum at 110 GeV and 130 GeV may not be manifested in the same regions of the instrumental variables, and so may not add coherently.

Unfolded distributions of incidence angles are shown

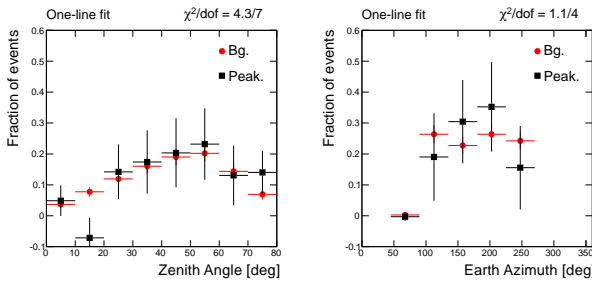


FIG. 7: Disentangled signal and background distributions. Left, angle between the reconstructed photon direction and the zenith line, which passed through the earth and Fermi's center of mass. Right, the earth azimuth angle.

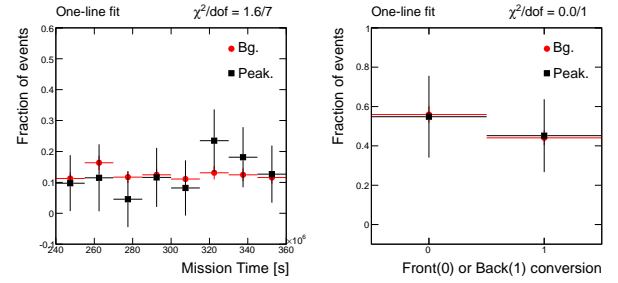


FIG. 8: Disentangled signal and background distributions. Left, the mission elapsed time since Jan 1 2001 [13]. Right, fraction of events in which the pair production is induced in the front (thin) or back (thick) layers of the tracker.

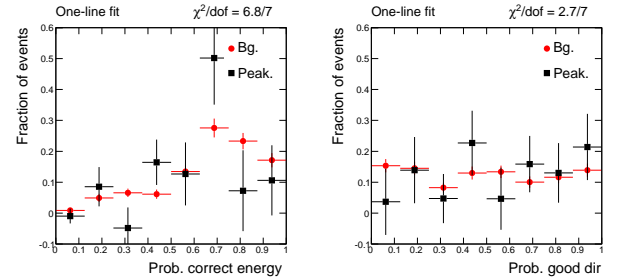


FIG. 9: Disentangled signal and background distributions. Left, probability of correct energy reconstruction. Right, probability of correct angle reconstruction.

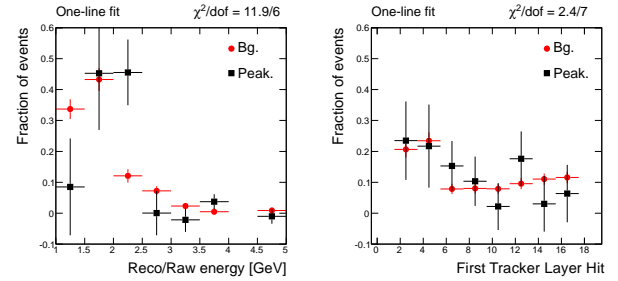


FIG. 10: Disentangled signal and background distributions. Left, ratio of reconstructed to raw photon energy. Right, the first layer of the tracker with a hit.

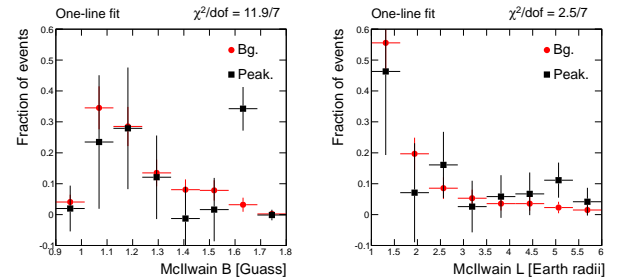


FIG. 11: Disentangled signal and background distributions. Left, magnetic field strength in terms of the Mclwain B parameter. Right, the Mclwain L parameter.

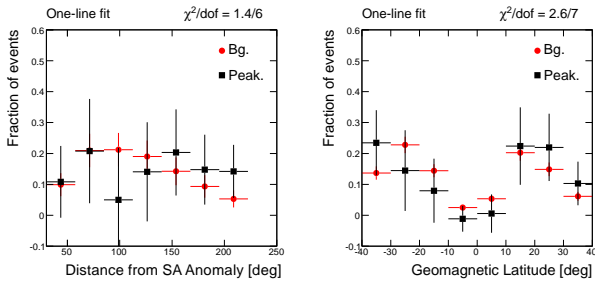


FIG. 12: Disentangled signal and background distributions. Left, the distance in Earth longitude and latitude from the center of the South Atlantic Anomaly. Right, geomagnetic latitude of the spacecraft.

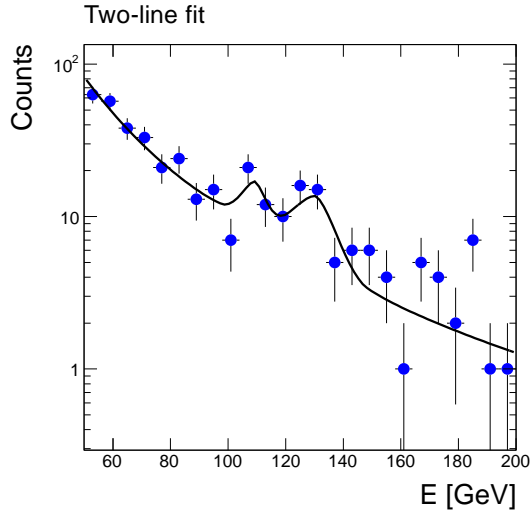


FIG. 13: Energy of Fermi-LAT photons with signal plus background fit in the double-line analysis at $E_\gamma = 110$ GeV and $E_\gamma = 130$ GeV.

in Fig. 14. The distributions in galactic coordinates can be seen in Fig. 15. Zenith and azimuthal angle distributions are in Fig. 16, and the recorded time and conversion type are in Fig. 17. Energy and direction reconstruction quality are in Fig. 18 and the reconstructed/raw energy ratio as well as the first layer of the tracker with a hit are shown in Fig. 19. The magnetic field parameters are shown in Fig. 20 and the distance from the South Atlantic anomaly and the geomagnetic latitude are shown in Fig. 21. In each case, we compare the distributions quantitatively by calculating the χ^2/dof between the peak and background distributions, shown in Table I.

SENSITIVITY

The number of events in the observed peak is not large, which makes the task of identifying a potential instrumental feature difficult. Before we can draw con-

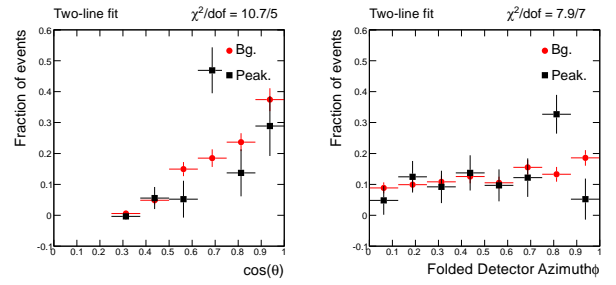


FIG. 14: Disentangled signal and background distributions in the double-line analysis. Left, $\cos(\theta)$ where θ is the photon incidence angle relative to a line normal the Fermi-LAT face. Right, ϕ , the photon incidence angle relative to the sun-facing side [13].

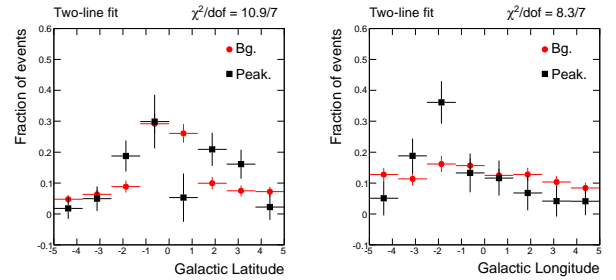


FIG. 15: Disentangled signal and background distributions in the double-line analysis in galactic coordinates, b (latitude) and l (longitude) [13]. No smoothing has been applied.

clusions about the distributions above, we must understand whether we would expect to see a feature given the current statistics.

To probe this question, we perform simulated experiments using a hypothetical variable in which the background is uniformly distributed between 0 and 1 and the signal peak is a delta function at 0.45; this represents an optimistic scenario in which the entire signal is tightly clustered. Figure 22 shows representative individual ex-

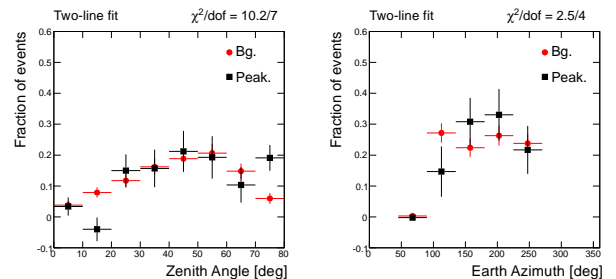


FIG. 16: Disentangled signal and background distributions in the double-line analysis. Left, angle between the reconstructed photon direction and the zenith line, which passed through the earth and Fermi's center of mass. Right, the earth azimuth angle.

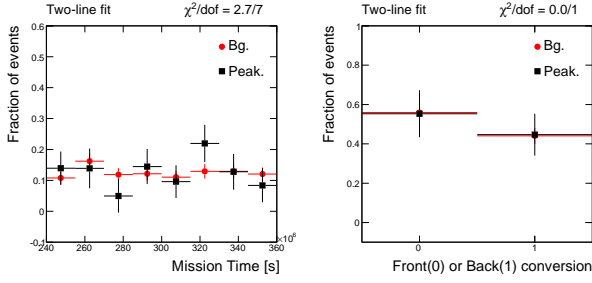


FIG. 17: Disentangled signal and background distributions in the double-line analysis. Left, the mission elapsed time since Jan 1 2001 [13]. Right, fraction of events in which the pair production is induced in the front (thin) or back (thick) layers of the tracker.

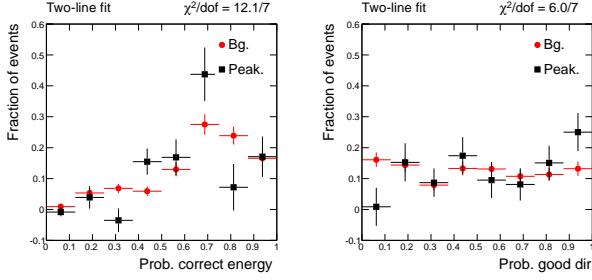


FIG. 18: Disentangled signal and background distributions. Left, probability of correct energy reconstruction. Right, probability of correct angle reconstruction.

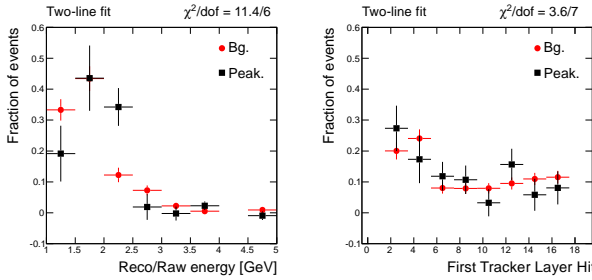


FIG. 19: Disentangled signal and background distributions. Left, ratio of reconstructed to raw photon energy. Right, the first layer of the tracker with a hit.

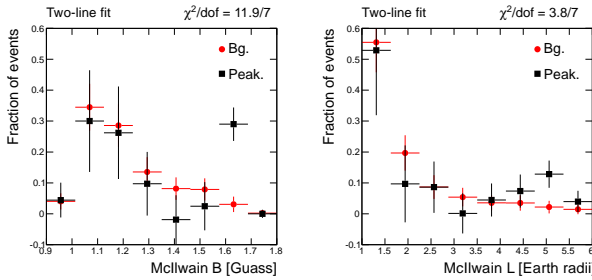


FIG. 20: Disentangled signal and background distributions. Left, magnetic field strength in terms of the McIlwain B parameter. Right, the McIlwain L parameter.

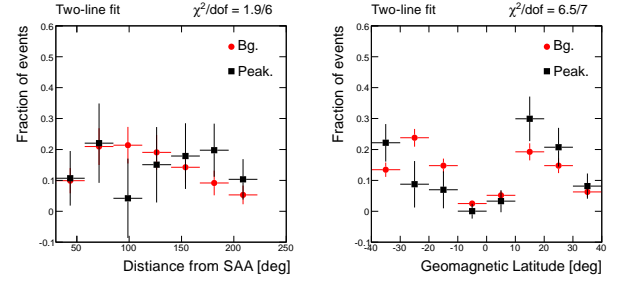


FIG. 21: Disentangled signal and background distributions. Left, the distance in Earth longitude and latitude from the center of the South Atlantic Anomaly. Right, geomagnetic latitude of the spacecraft.

TABLE I: Summary of consistency between background and peak distributions for each of the considered instrumental variables, expressed as the χ^2 per degree of freedom.

Variable	Single-line	Double-line
	χ^2/dof	χ^2/dof
$\cos(\theta)$	8.9/5	10.7/5
Detector Azmith	4.4/7	7.9/7
Zenith Angle	4.3/7	10.2/7
Earth Azimuth	1.1/4	2.5/4
Mission Time	1.6/7	2.7/7
Conversion Type	0.0/1	0.0/1
Prob correct energy	6.8/7	12.1/7
Prob correct dir	2.7/7	6.0/7
Reco/Raw energy	11.9/6	11.4/6
First tracker hit	2.4/7	3.6/7
McIlwain B	11.9/7	11.9/7
McIlwain L	2.5/7	3.8/7
Distance from SA Anomaly	1.4/6	1.9/6
Geomagnetic Latitude	2.6/7	6.5/7

ample experiments with either zero, 12 or 100 signal events. If the signal statistics were very large ($N_{\text{sig}} = 100$ events), such a strong feature would be observable both as a discrepant single bin and a $\chi^2/\text{d.o.f.}$ with low probability, $P(\chi^2/\text{d.o.f.} = 34.6/7) = 10^{-5}$. In the current statistics ($N_{\text{sig}} \approx 12$ events), the feature would be noticeable in a single bin, but the $\chi^2/\text{d.o.f.}$, which analyzes the global consistency of the two distributions, would be reasonable, $P(\chi^2/\text{d.o.f.} = 7.7/7) = 0.36$.

In the instrumental features we study here, this scenario may be overly optimistic – a real instrumental feature may appear as a more subtle difference between the two distributions. It may also be pessimistic, as the signal feature could appear where the background is suppressed, whereas in the hypothetical variable the background is uniform. However, the simulated experiments suggest that even if there were a true strong instrumental disagreement between the signal-like and background-like photons, we may identify one or two discrepant bins, but are unlikely to find a χ^2/dof with convincingly small probability. This emphasizes our earlier point, that an

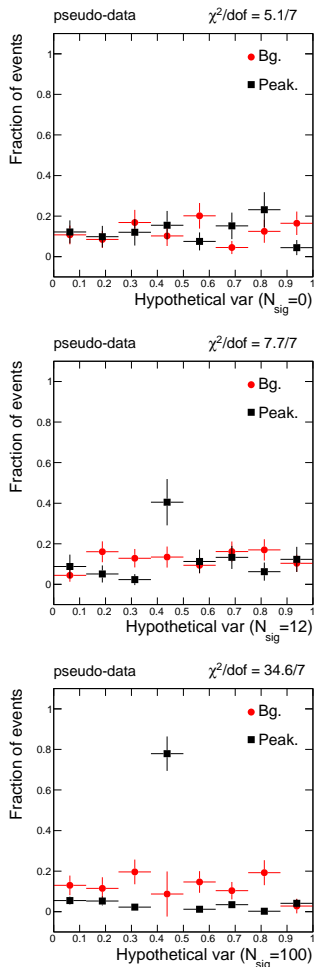


FIG. 22: Disentangled signal and background distributions in simulated experiments hypothetical variable in which the background is uniform and the signal is a delta function at $x = 0.45$, for varying amounts of signal. Top, no signal events; center, 12 signal events, the approximate number seen in the Fermi-LAT data; bottom, 100 signal events.

observed discrepancy in the distribution of signal-like and background-like photons should serve as a clue for further instrumental studies, rather than conclusive evidence for or against an instrumental explanation.

As a positive control, we can examine the galactic longitude. The feature at $E_\gamma = 130$ GeV has been previously localized to $l = -1.5^\circ$ [6], which is consistent with what we observe in Fig 6. While the individual bin near $l = -1.5^\circ$ shows a large discrepancy between signal-like and background-like photons, the global agreement of the distributions in longitude is reasonable, with a p -value of 0.3.

DISCUSSION

Examining the unfolded distributions, there are several bins which show suggestive but inconclusive discrepancies. The distribution of $\cos(\theta)$ (Fig. 5) shows a bin with a large fraction of the signal events near $\cos(\theta) = 0.7$. This is unlikely to cause a feature in the energy spectrum, though the resolution depends on $\cos(\theta)$, as the cluster occurs at the median value rather than at either extreme. The overall consistency is reasonable, $P(\chi^2/\text{d.o.f.} = 8.9/5) = 0.11$, though see the sensitivity discussion above. Similarly, there is a single discrepant bin in the McIlwain B parameter at 1.65 Gauss (Fig. 11). These may be useful clues for further instrumental studies.

CONCLUSIONS

We have performed an initial study of the instrumental characteristics of events from the feature at $E_\gamma = 130$ GeV observed in the Fermi-LAT data.

In the instrumental variables available in the public data distribution, we find no conclusive difference in characteristics between peak photons and background photons, see Table I. There are several suggestive discrepancies, near $\cos(\theta) = 0.7$ or McIlwain B parameter of 1.65 Gauss which deserve further study by instrumental experts.

There are several additional instrumental variables which should be examined, such as the incident position on the face of the LAT, but are not available in the public data.

If a striking feature had appeared – such as a clustering of the peak photons at a given time or near a specific angle of incidence – it would have pointed to an instrumental issue. The statistics of the sample are too poor to draw strong conclusions, but the lack of a very clear features makes an instrumental explanation somewhat less likely.

ACKNOWLEDGEMENTS

DW acknowledges contributions, explanations and useful discussions with Eric Albin which are clearly deserving of authorship, comments from Aaron Pierce, Paddy Fox and Tim Tait, insightful statistical comments from Kyle Cranmer, and technical support from Mariangela Lisanti and Tracy Slatyer. DW is supported by grants from the Department of Energy Office of Science and by the Alfred P. Sloan Foundation. DW is grateful to the Aspen Center for Physics, where this work was performed and supported by NSF grant no. 1066293.

-
- [1] A. A. Abdo *et al.* [The Fermi-LAT Collaboration], Phys. Rev. Lett. **104**, 091302 (2010) arXiv:1001.4836
- [2] M. Ackermann *et al.* [Fermi-LAT Collaboration], (2012), arXiv:1205.2739
- [3] T. Bringmann, X. Huang, A. Ibarra, S. Vogl and C. Weniger, (2012), arXiv:1203.1312
- [4] C. Weniger, (2012), arXiv:1204.2797
- [5] E. Tempel, A. Hektor and M. Raidal, (2012), arXiv:1205.1045
- [6] M. Su and D. P. Finkbeiner, (2012), arXiv:1206.1616
- [7] T. Cohen, M. Lisanti, T. R. Slatyer and J. G. Wacker, (2012), arXiv:1207.0800
- [8] M. Pivk and F. R. Le Diberder, Nucl. Instrum. Meth. A **555**, 356 (2005) physics/0402083
- [9] INSPIRE search for “refersto:recid:644725” yields no items posted to astro-ph.
- [10] Pass7, `ultraclean` class, quality requirements: `DATA_QUAL= 1 && LAT_CONFIG=1 && ABS(ROCK_ANGLE)≤52 && ZENITH<100` and a good time interval (via `gtmktime`).
- [11] [Fermi-LAT Collaboration], arXiv:1206.1896 [astro-ph.IM].
- [12] <http://fermi.gsfc.nasa.gov/ssc/data/analysis/documentation/>
- [13] <http://fermi.gsfc.nasa.gov/ssc/data/analysis/documentation/>
- [14] McIlwain, C. E., J. Geophys. Res. 66, pp. 3681-3691 (1961).
- [15] W. B. Atwood *et al.* [LAT Collaboration], Astrophys. J. **697**, 1071 (2009) [arXiv:0902.1089 [astro-ph.IM]].
- [16] A. A. Abdo *et al.* [Fermi LAT Collaboration], Astropart. Phys. **32**, 193 (2009) [arXiv:0904.2226 [astro-ph.IM]].
- [17] A. Rajaraman, T. M. P. Tait and D. Whiteson, JCAP, accepted (2012), arXiv:1205.4723.